Impuls- und Vernetzungsfonds

Zwischenbericht 2014

Förderprogramm:	**Virtuelle Institute**
Impulsfonds-Projektnummer:	VH-VI-403
Projekttitel:	In-Situ Nano-Imaging of Biological and Chemical Processes
Federführende/r Wissenschaftler/in	Christian Schroer
Berichtszeitraum (Förderungszeitraum)	01.01.2014 – 31.12.2014

Sachbericht

1 Fortschritt des im Antrag beschriebenen Arbeitsprogramms

In the framework of this VI, the following sub-projects have been addressed during the year 2014:

- 1.1 Combined Ptychography and Nano Diffraction for Cellular Imaging (AG Köster & AG Schroer)
- 1.2 Imaging of in Vitro Assembled Keratin Protein Bundles by X-ray Nano Diffraction (AG Köster)
- 1.3 Ultra-fast Membrane Dynamics (AG Salditt)
- 1.4 Holographic Live Cell Imaging (AG Salditt)
- 1.5 X-ray Microprobe Analysis of Melanosomes (AG Rosenhahn)
- 1.6 Morphological Fingerprinting of Antimicrobial Modes of Action (AG Rosenhahn)
- 1.7 Imaging Catalysts at the Meso Scale: Observation of Gradients During the Catalytic Partial Oxidation of Methane (AG Grunwaldt)
- 1.8 *In-situ* Ptychography (AG Grunwaldt & AG Schroer)
- 1.9 Instrumentation, Dissemination of Methods and User Experiments on *In-Situ* Chemical and Biological Processes (AG Salditt)
- 1.10 Combining Droplet Microfluidics and SAXS to Track Reactions in Picoliter Compartments (AG Köster)
- 1.11 Implementation of a New Sample Stage for HORST (AG Rosenhahn)
- 1.12 A Micro-Patterned Silicon Chip as Sample Holder for Macromolecular Crystallography Experiments with Minimal Background Scattering (AG Meents)

- 1.13 Hard X-ray Nanofocusing by Refractive Lenses of Constant Thickness (AG Schroer)
- Ptychographical imaging of the phase vortices in the X-ray beam formed by nanofocusing lenses (AG Vartanyants & AG Schroer) [1]

Some these sub-projects are described in more detail below.

1.1 Combined Ptychography and Nano Diffraction for Cellular Imaging (AG Köster & AG Schroer)

Imaging cells at high spatial resolution and ideally little required sample preparation is highly desired for the investigation of biological processes. We have combined two modern x-ray imaging techniques, namely ptychography and nano-diffraction in order to obtain both high-resolution real space images and structural information from certain regions of interest in the cells.

Cells were grown on Si_3N_4 windows, chemically fixed and freeze-dried [28], [2]. We performed the ptychography measurements at a sample position 1 mm out of focus to obtain a large enough beam of 850×950 nm^2 to minimize the number of scan positions required and thus the dose imposed on the sample ($D = 1.3 \times 10^6$ Gy per scan point). The detector distance was 2.2 m, no beam stop was employed and flux was reduced by closing the vertical and horizontal slits. The nano-diffraction ($D = 3 \times 10^8$ Gy per scan point and a beam size of 100×150 nm^2), by contrast, was performed in focus at a detector distance of 1 m with beam stop [3].

We observed a dense and highly structured network (see Fig. 1a), which we identified as the keratin network in these cells [28, 29], [2]. In nano-diffraction with a small step size of 100 nm and 1 s exposure time per scan point, the network is directly visible (Fig. 1c) and corresponds well to the ptychography image (corresponding region shown in Fig. 1d). Each scan position in Fig. 1c contains a complete 2D scattering signal (for an example of such a single diffraction pattern see Fig. 1d). These patterns are highly anisotropic and when azimutally integrated (Fig. 1f) characteristic modulations are observed.

Thus, we were able to demonstrate the feasibility and the advantages of such a combined ptychography/nano-diffraction imaging approach for subcellular components. By combining high-resolution imaging in real and in reciprocal space, we obtain quantitative structural information on many length scales, providing a wealth of information about the system. The technique used here will in the future be applicable to other biological and soft matter systems.

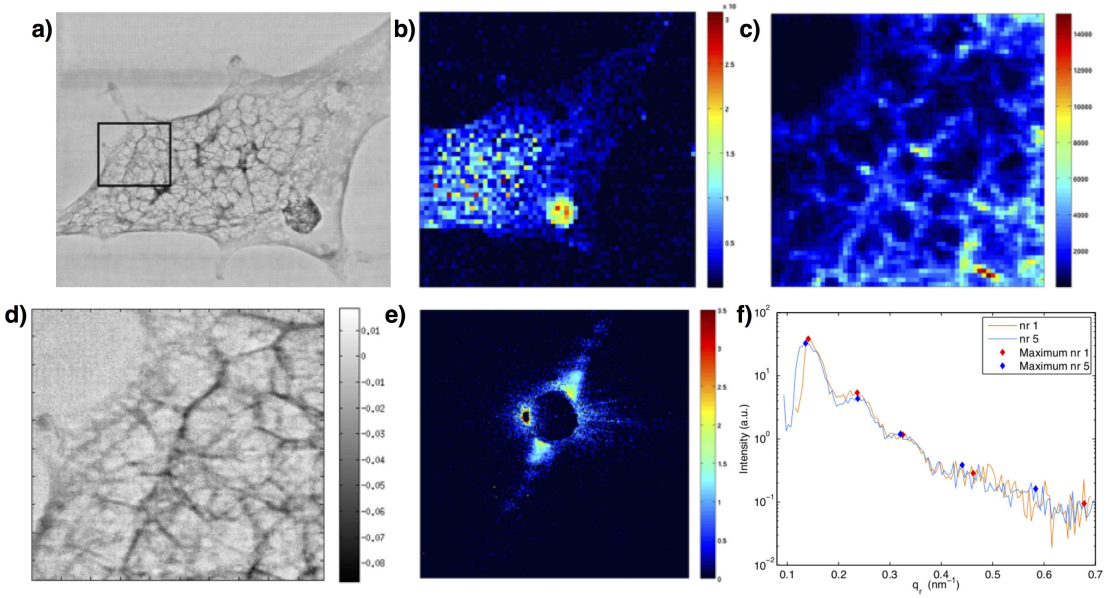

Figure 1: a) Ptychogram of one cell; 100 × 100 scan points, step size 300 nm, exposure time 40 ms per scan point. b) Coarse nano-diffraction scan, dark-field representation, of the same cell. c) Fine nano-diffraction scan of the ROI highlighted in a), exposure time per scan point 1 s, 100 nm step size. d) Detail of the ptychogram corresponding to the region shown in c). e) One individual diffraction pattern showing strong anisotropy. f) Azimuthally integrated intensity plotted over the scattering vector q.

1.2 Imaging of in Vitro Assembled Keratin Protein Bundles by X-ray Nano Diffraction (AG Köster)

Keratin proteins belong to the intermediate filament (IFs) protein family that constitutes the cytoskeleton of eukaryotes together with actin filaments and microtubules. In cells, keratin bundles (laterally associated, packed filaments) provide a prime biophysical example of a highly ordered natural structure. Epithelial cells are continuously exposed to pressures and shear forces and these impacts are to a great part being born by the keratin network within the cells. We formed the bundles by adding multivalent ions to the keratin [30] and used a nano- or micro-focused beam (ID13) to locally probe the structure, orientation and characteristic length scales of the material. We have previously measured keratin in whole, freeze-dried, chemically fixed, or living cells [28, 29], [2] and could relate the signal to these keratin structures; however, investigating a corresponding purified system will help to better understand and "calibrate" the signal we have measured in cells.

In vitro keratin bundles/networks complemented with salt were investigated. The protein was assembled on silicon nitride (Si_3N_4) or TOPAS (a cyclic olefin copolymer) films by droplet-fusion technique. Bundles were localized using the online microscope of the

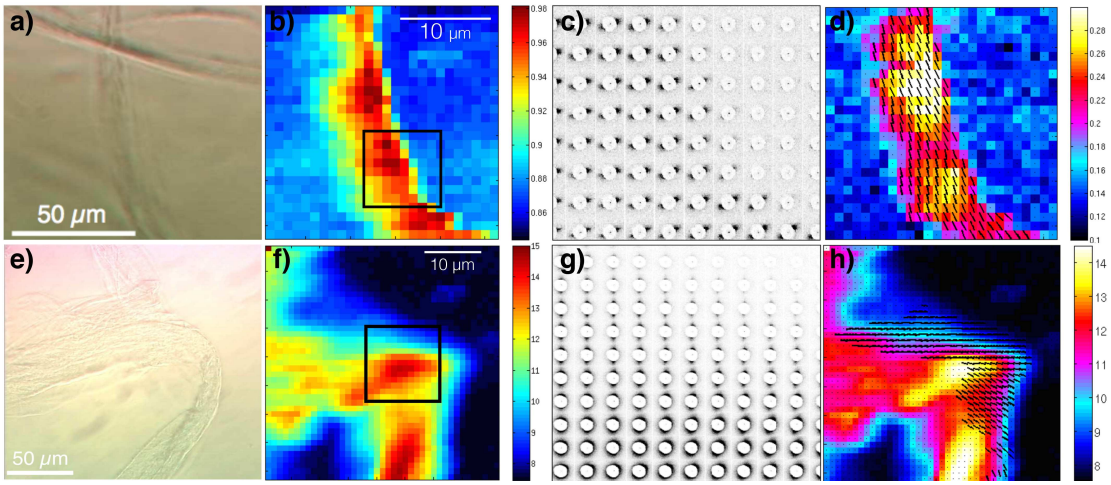

Figure 2: Micro-beam results a) Online micrograph of keratin bundles assembled with 20 mM KCl. b) Dark-field representation, of the same bundle. c) Composite images of the previous black square from b) showing anisotropy of the signal. d) Orientation (vectors) and degree of anisotropy (colormap). e) Online micrograph of keratin bundles assembled with 1 mM $MgCl_2$. f) Dark-field representation, of the same bundle. g) Composite images of the previous black square from f) showing some anisotropy of the signal. h) Orientation (vectors) and degree of anisotropy (colormap).

beamline (Fig. 2a and e), and we then scanned the sample through the beam.

Using the microbeam, we could record dark-field images of the bundles (Fig. 2b and f) and detect anisotropic scattering signal from single diffraction patterns (Fig. 2c and g). We analyzed the data to find the orientation of the local structures and the degree of anisotropy (Fig. 2d and h).

With the data analysis lined out above, we are confident to be able to show structural changes induced by different ions and different concentrations (see Fig. 2a-d for one example of keratin bundles assembled in the presence of 20 mM KCl and Fig. 2e-h for keratin assembled in the presence of 1 mM $MgCl_2$). One can see that in presence of 20 mM KCl the anisotropy of the signal is present for each scan point (Fig. 2c), which is not the case for the sample assembled in the presence of 1 mM $MgCl_2$ (Fig. 2g), especially in the denser parts of the dark-field image (high intensity, shown in red in Fig. 2f). Moreover, filaments look thicker for this concentration of magnesium as compared as the sample with potassium. This aspect could explain the loss of anisotropy, which is in fact averaged over several local orientations. Further analysis such as the 1D azimuthally integrated data will reveal the internal structure (e. g., form and structure factors such as cylinders packed into a hexagonal lattice) of the bundles. Further experiments at the micro-branch of ID 13 will be necessary for a comprehensive study of the structures evolving in keratin in the presence of different species and concentrations of ions.

1.3 Ultra-fast Membrane Dynamics (AG Salditt)

The membrane as nature's most important interface is constantly subjected to external forces, for example due to osmotic pressure differences, the coupling to an active cytoskeleton, or to membrane proteins such as ion channels or pumps. These effects may change structural, dynamical and mechanical properties on a fundamental level, but are extremely challenging to track down. For a simple reason: biomolecules are by nature very mobile, and even without external forces they vibrate, turn and stretch considerably at ambient temperature. Because these movements constantly overlap, the membrane structure and dynamics can in most cases be experimentally determined only as an average. In order to directly track the molecular dynamics, both the spatial and the temporal resolution have to be matched to molecular scales, and the excitation of membrane modes has to be synchronized to the probing picosecond X-ray pulses. Using time resolved X-ray diffraction under the favourable conditions of 192 ns bunch spacing at the PETRA III storage ring (40 bunch mode) in stroboscopic illumination, it became now possible to study out-of-equilibrium structural dynamics of lipid membranes, driven by surface acoustic waves for well controlled excitation. The results show that the internal bilayer structure begins to oscillate in response to the excitation. This work was published in T. Reusch et al. [4]. Associated technical work was published in [31] and [5, 6].

1.4 Holographic Live Cell Imaging (AG Salditt)

According to the project milestones, live-cell imaging has been a major effort. It has been achieved by the consortium in form of nano-beam diffraction and scanning transmission X-ray microscopy [2], live-cell imaging has now also been realized in form of the full-field holographic propagation imaging. Nanoscale X-ray holographic imaging was implemented using the optimized illumination wave fronts emitted by X-ray waveguide channels. High spatial coherence by mode filtering enables a quantitative reconstruction of the projected density, as first evidenced by imaging test patterns at 22 nm resolution. The dose efficiency and contrast sensitivity make the optical scheme compatible with samples of intrinsically low contrast, typical for hydrated soft matter. This was then demonstrated by imaging bacteria in the hydrated and living state, with quantitative phase contrast revealing dense structures in the interior of the bacteria. In response to continued irradiation, characteristic changes in these dense structures were observed. This work has been published in [7].

1.5 X-ray Microprobe Analysis of Melanosomes (AG Rosenhahn)

Mammalian melanin exists in two chemically distinct forms, black to brown eumelanin and yellow to reddish-brown pheomelanin [32]. In addition to contributing to the color of tissues, the differing physiochemical properties of eumelanin and pheomelanin —

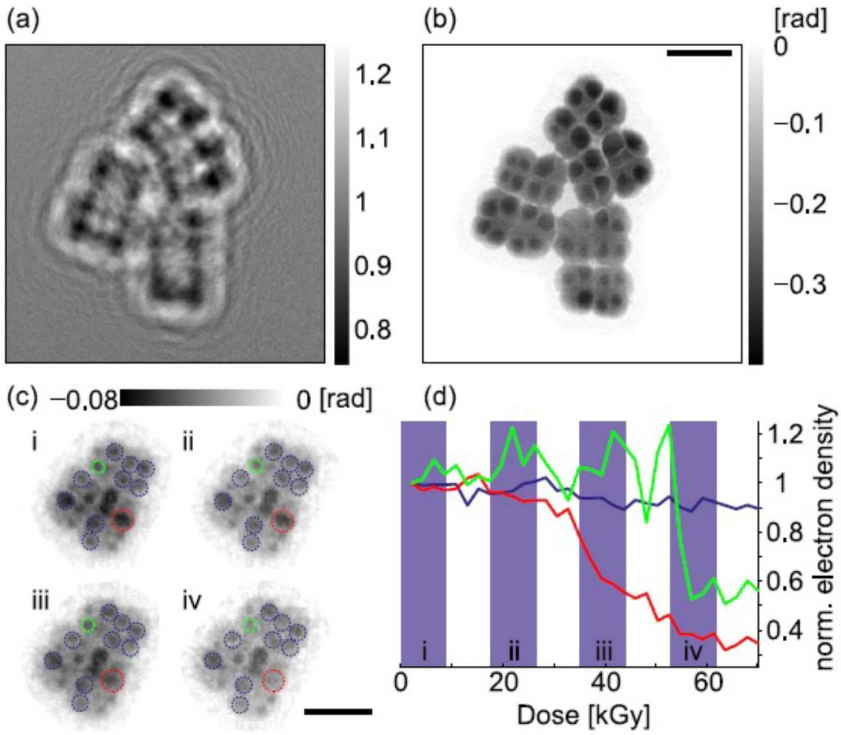

Figure 3: (a) Normalized hologram of freeze-dried *Deinococcus radiodurans* cells, obtained in a single recording with 8 s dwell time along with (b) the iterative mHIO phase reconstruction. (c) mHIO reconstruction of (initially) living cells in solution. Each frame was accumulated for 8×10 seconds (every other frame is shown). Pronounced changes in the densities are observed after successive irradiation, as quantified in (d), showing the normalized electron density in the high density regions indicated by the corresponding colors as a function of dose. The images in (c) are reconstructions corresponding to averages over the colored columns in (d).

especially their opposing anti-oxidant and pro-oxidant natures — likely influence several diseases [33]. While their distribution has been studied extensively within whole tissues [34], the spatial organization of eumelanin and pheomelanin at the level of melanosomes has been more difficult to investigate. Based on biochemical findings, a 'casing model' that predicts individual melanosomes to contain a pheomelanin core surrounded by a eumelanin shell was proposed [35]. Since then, additional support for the casing model has come from two primary sources: predictions based on the intrinsic chemical reactivity of orthoquinones [36] and direct measurements of surface ionization thresholds of melanin [37]. Thus, while the model is widely accepted, it has also been somewhat recalcitrant to other forms of direct experimentation that might challenge or confirm it.

X-ray fluorescence (XRF) analysis with synchrotron radiation allows visualization of metals at the nanoscale by irradiating a sample region with focused X rays and detecting

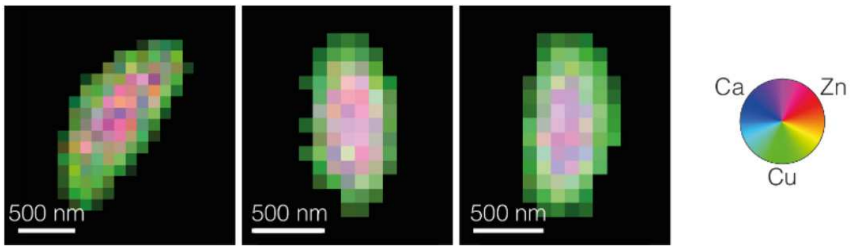

Figure 4: Direct visualization of the melanosomal casing model by means of X-ray fluorescence nanoimaging.

emitted fluorescence photons characteristic for specific elements. Thus, XRF studies of Cu distribution in melanosomes offer a new opportunity for testing the casing model, and at the same time allow the distribution of other metals within melanosomes to be discovered at sub-100 nm resolution. To apply XRF analysis to melanosome samples, iridial melanosomes from inbred strains of mice were prepared (vitrified and subsequently freeze-dried) and studied using the ID22NI end-station of the European Synchrotron Radiation Facility (ESRF) in Grenoble, France [38].

Results of this experiments showed robust signatures for copper (Cu), calcium (Ca), and zinc (Zn). Analysis of Cu, Ca, and Zn shows variable concentrations and distributions, with Ca/Zn highly correlated, and at least three discrete patterns for the distribution of Cu vs. Ca/Zn in different melanosomes – including one with a Cu-rich shell surrounding a Ca/Zn-rich core. Thus, the results support predictions of the casing model, but also suggest that in at least some tissues and genetic contexts, other arrangements of melanin may co-exist [8].

1.6 Morphological Fingerprinting of Antimicrobial Modes of Action (AG Rosenhahn)

The emergence of multi-drug resistant microbes creates an urgent demand for new antibiotic substances [39]. In order to be effective against such pathogens, drugs with a new mode of action are desired. Despite massive substance screening efforts by both, universities and pharmaceutical industry, antibiotics with a truly novel mechanism of action are particularly difficult to find [40]. Even though huge numbers of antimicrobial compounds can be developed, it takes substantial time and resources to determine whether a candidate substance has a new mode of action and is therefore worth further investigations. As the bacterial morphology is affected by antibiotic action the working hypothesis was to apply small angle X-ray scattering as a structure sensitive tool to obtain nanoscale information averaged over a large number of cells. The intriguingly short acquisition times (≈ 1 s) have fostered the optimization of automated sample delivery systems. As a result, technologically matured SAXS experiments can operate in a high-throughput fashion [41].

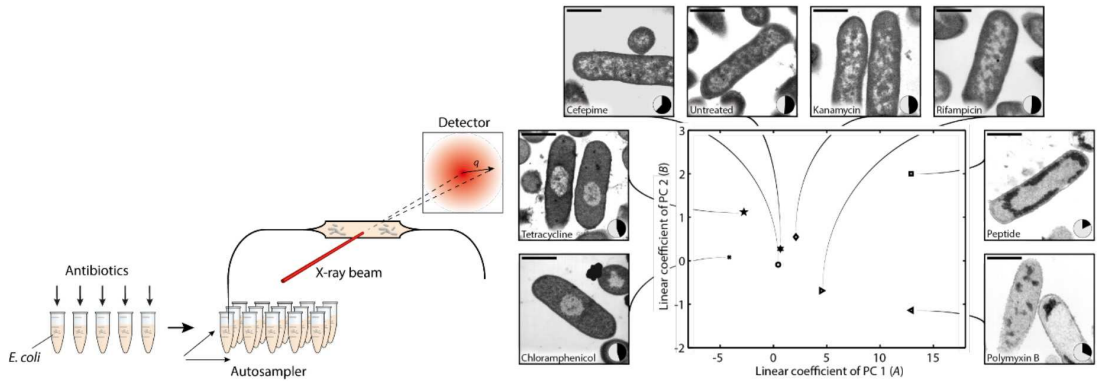

Figure 5: Scheme of the high-throughput SAXS experiment. *E. coli* cells were treated with antibiotics. At the BioSAXS beamline (P12, EMBL/DESY) at PETRA III, Hamburg) the sample is collected by an autosampler and injected into a capillary to perform the SAXS experiment. b) The linear coefficients A and B of the principal component analysis discriminate the morphological changes in *E. coli* cells induced by antibiotics. A correlation with TEM images visualize the observed changes.

For these proof-of-principle experiments, *Escherichia coli* were treated with a selection of antibiotics including clinically relevant antibiotics and a short cationic peptide as a member of novel promising substance class [42]. The SAXS experiments were performed on the BioSAXS beamline P12 at PETRA III (in coll. with Helmholtz-Center Geesthacht). In order to find neutral descriptors of the morphological change we processed the scattering curves with a principal component analysis. As a result we were able to classify protein synthesis inhibitors, RNA-synthesis inhibitors, membrane disrupting antibiotics, and the short cationic peptide due to their impact on the bacterial morphology. Additionally the growth state of untreated *E. coli* could be monitored. Since both the technique and the analysis can be performed rapidly, we envision SAXS as future key tool within the high-throughput screening pipeline of modern drug discovery.

1.7 Imaging Catalysts at the Meso Scale: Observation of Gradients During the Catalytic Partial Oxidation of Methane (AG Grunwaldt)

Understanding the function of catalysts requires knowledge on different length scales [44]. Furthermore, the catalyst has to be studied during the catalytic reaction, i. e., under *in-situ* conditions [45]. Therefore, dedicated *in-situ* cells are needed [46]. Here, a lithographically fabricated microreactor for gas phase reactions is presented [43]. The reactor has been optimized by means of temperature homogeneity and has been furthermore tested for various characterization techniques such as X-ray absorption spectroscopy, X-ray diffraction, Raman spectroscopy and IR thermography. *In-situ* studies were performed during the catalytic partial oxidation (CPO) of methane, which is an

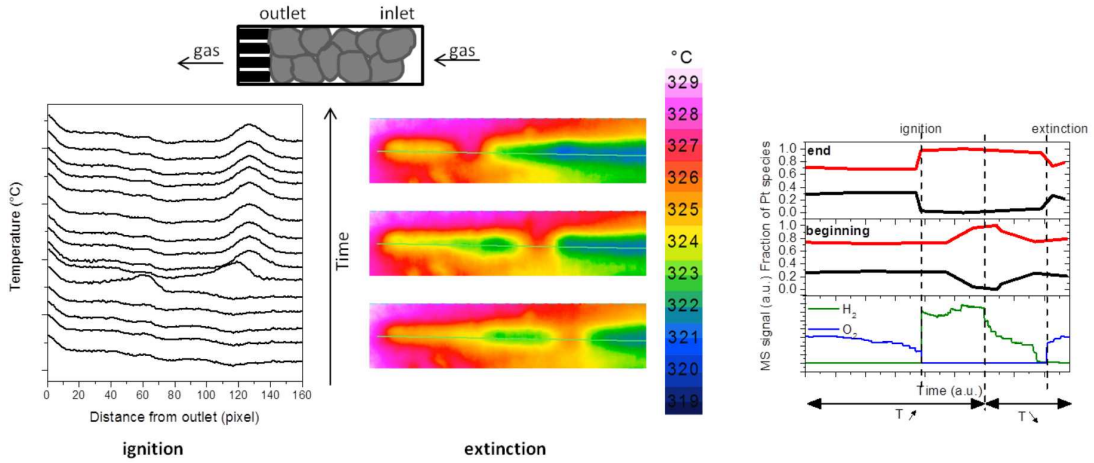

Figure 6: Left and middle: IR thermography visualizing the hotspot during the ignition and extinction of the catalytic partial oxidation of methane. Right: Mass spectrometry and fraction of Pt species during one catalytic cycle of the CPO of methane [43].

important small scale application for hydrogen production [47]. During the CPO, before ignition of the reaction, a hotspot can be detected. When the temperature is increased, this hotspot is shifted more towards the beginning of the catalytic bed. During extinction of the reaction, the hotspot moves in the opposite direction of the reactor towards the end of the catalytic bed [48]. As the hotspot moves stepwise, we assume influences of the single catalyst grains, which have to be studied. In parallel to the appearing hotspot, the ignition of the reaction can be followed by mass spectrometry monitoring the production of hydrogen. Performing spatially resolved XAS measurements in parallel, one could observe a gradient in oxidation state along the reactor from a more reduced state at the outlet towards the end of the catalytic bed to a more a more oxidized state at the inlet of the reactor. With changing temperature, also this gradient moves in position. The movement of the hotspot as well as the gradient in oxidation state inside the microreactor are shown in Fig. 6. With this microreactor, due to the small channel design with a thickness of 250 μm, spatially resolved XAS can lead to high resolution information on single grains. To study such effects, a microfocusd beam spot or full field imaging enabling high resolution is required. Up to now, no beamtime was allocated for such single grain studies, yet.

Furthermore, recently the number of relevant reactions were extended especially in the field of exhaust gas catalysis. On the one hand spatially resolved studies during the selective catalytic reduction of NO by ammonia were conducted and strong changes were found along the microreactor like in the case of the catalytic partial oxidation of methane [9]. In addition, oscillatory CO oxidation was conducted and strong oscillations both with respect to catalytic activity (hotspot formation) and structure (oxidation/reduction) were found [49]. In other studies, quasi *in-situ* tomography during ageing of an exhaust

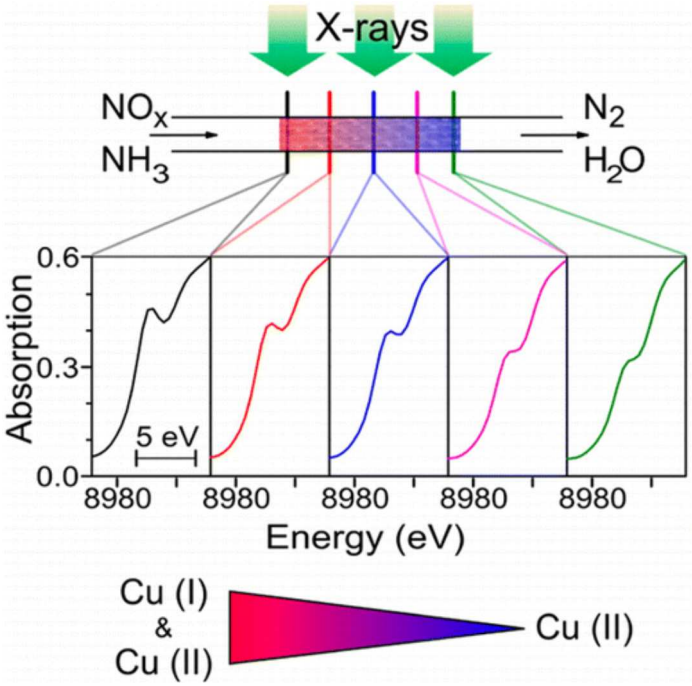

Figure 7: XANES spectra at Cu K-edge of the Cu-SAPO-34 catalyst during NH_3 oxidation and NO oxidation at 255 °C. The spectra are measured at the different points of the microreactor (5 points, from inlet to outlet in the direction of arrow). Conditions: 1000 ppm NO, 800 (top) or 1200 (bottom) ppm NH_3, 10%O_2, 1.5% H_2O, He balance; GHSV = 360 000 h^{-1}.

gas catalyst was conducted [10], [50].

1.8 *In-situ* Ptychography (AG Grunwaldt & AG Schroer)

Studying catalysts does not only require spatially resolved spectroscopy on the meso scale, but also imaging techniques from the meso to nano range [44]. Although electron microscopy results in higher resolution for imaging techniques, it is mostly restricted to image acquisition at low pressures [51]. However, in order to optimize catalytic processes and to understand for example catalyst aging, which can be caused by sintering, studies have to be performed under realistic conditions *in situ* [52, 53]. To exploit the complementary information gained by high-resolution electron microscopy and by *in-situ* X-ray microscopy, a cell suitable for hard X-ray ptychography has been developed in collaboration with DTU [54]. This cell has been used for the first time for *in-situ* ptychography during annealing treatment of gold particles (Fig. 8) and nanoporous gold catalysts (Fig. 9; collaboration with University of Bremen). In Fig. 8, the change of the overall shape of the agglomeration of gold particles due to sintering is clearly visible.

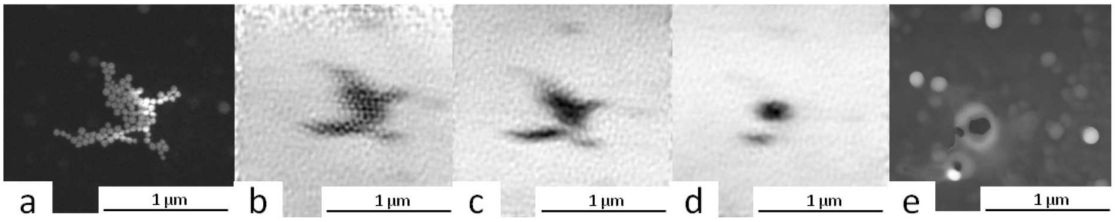

Figure 8: Annealing study of 50 nm gold particles by means of scanning electron microscopy (SEM) and hard X-ray ptychography (phase contrast). A) *Ex situ* (vacuum) SEM image before heating in synthetic air, b) ptychographic reconstruction before heating inside the cell within a flow of synthetic air c) ptychographic reconstruction after the first annealing treatment, d) ptychographic reconstruction after the second annealing treatment at higher temperature, e) *ex situ* SEM image after being used in the cell.

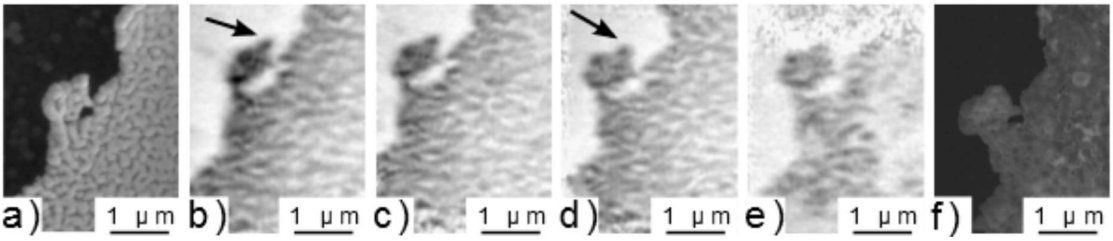

Figure 9: Annealing study of CeO_2 supported nanoporous gold by SEM and hard X-ray ptychography. a) SEM image (vacuum) before heating, b) ptychographic reconstruction before heating inside the cell within a flow of synthetic air c-e) ptychographic reconstruction during the annealing steps at increased temperature within a flow of synthetic air f) SEM image after being used inside the cell.

For a "proof of principle", images were recorded after heating when the sample was cooled down. Besides, *in-situ* measurements at elevated temperature and in controlled atmosphere have for example been gained for CeO_2 supported nanoporous gold catalysts shown in Fig. 9. Changes appeared at relatively low temperature and are marked by arrows. For comparison, the samples have been studied by electron microscopy before and after the reaction (collaboration with KNMF). To conclude, *in-situ* ptychography measurements with a resolution around 30 nm revealed the applicability of the cell for such *in-situ* studies and show better resolution than recently published work by other groups [55, 53].

1.9 Instrumentation, Dissemination of Methods and User Experiments on In-Situ Chemical and Biological Processes (AG Salditt)

The long PETRA III shutdown was used to perform an upgrade of the GINIX nano-focus endstation (new KB mirror polishing, new optical stages, upgrade of optical microscopes

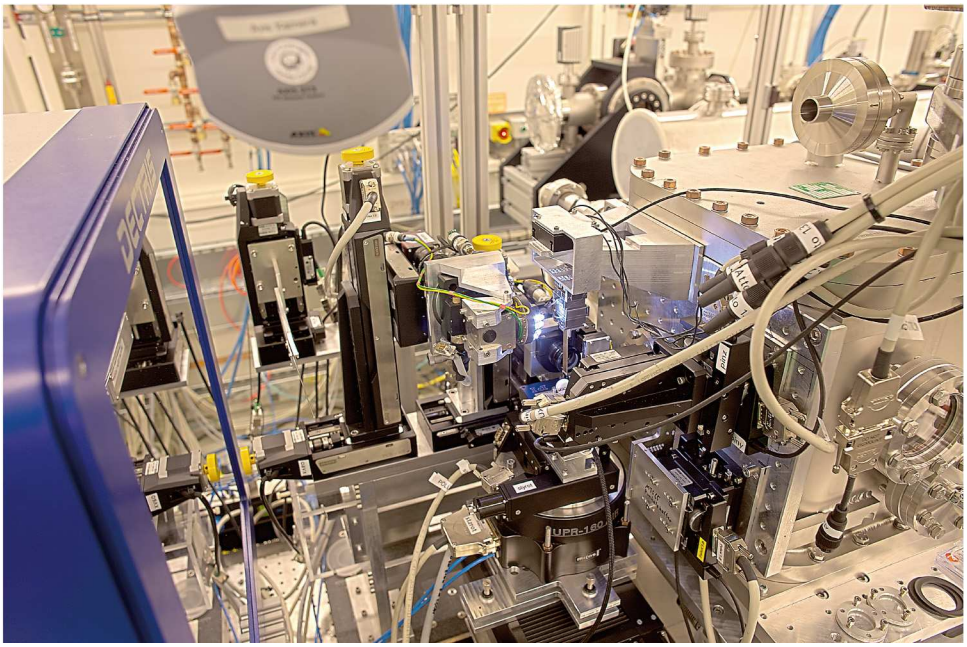

Figure 10: Setup for scanning WAXS using the Ginix/P10 nanofocus for time-resolved dynamic tracking of photo-induced structural changes in crystallites (Photo: M. Osterhoff).

for *in-situ* inspection in particular of non-static samples such as living cells). Furthermore, results obtained in different user experiments in the previous beamtime periods were analyzed and written up. Two applications are particularly worthwhile to mention here, since they relate to the heart of the present topic. Firstly, semiconductor nanowire samples were investigated by scanning diffraction and coherent imaging using the P10 nanofocus, while the nanowires were electrically contacted. In this way, I-V curves could be recorded during X-ray exposure. These results were published in [11]. More of these operando experiments are in planning.

Secondly, the group of John Miao, UCLA, carried out experiments together with the Salditt group at the Ginix/P10 beamline, investigating how crystallite grains change during a photo-reaction [12]. The combination of nanofocusing and wide angle diffraction in a time-resolved mode suitable to follow grain rotation and deformations dynamically was a particular instrumentation challenge, see Fig. 10.

1.10 Combining Droplet Microfluidics and SAXS to Track Reaction in Picoliter Compartments (AG Köster)

We studied the effect of monovalent salts on vimentin intermediate filament (IF) assembly (see also section 1.1) as well as the effect of divalent ion on aggregation of filaments

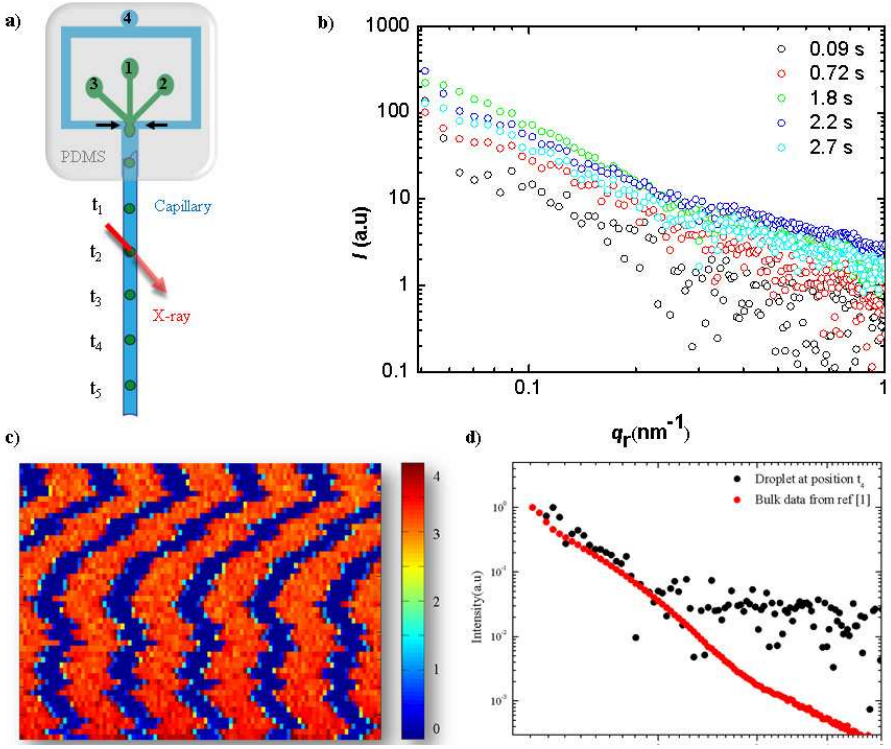

Figure 11: a) Sketch of the microfluidic channel geometry and the PDMS-capillary device for generating water-in-oil emulsions. b) Radially integrated SAXS curves of vimentin at different stages of the assembly process. c) Composite image of signal taken while one droplet flowed by the beam. The streaks coming from the droplet edges can be clearly seen. d) The radially integrated signal (black) was averaged over about 2500 exposures of 10 ms each from inside the drops and background corrected by the averaged signal from empty drops; the data are compared to bulk data (red) [13] at similar salt concentration.

into larger structures by SAXS in microflow. IFs, together with actin filaments and microtubules make up the cytoskeleton, which provides biological cells with their mechanical properties. Vimentin IFs are mainly found in cells of mysenchymal origin. The assembly from smaller subunits, namely tetramers, into extended, micrometer-long filaments occurs first laterally and then longitudinally [56]. We employed droplet microfluidics to encapsulate the assembled vimentin filaments. Bulk SAXS studies of vimentin filaments in the presence of mono- and divalent ions [13] had been performed previously in standard capillaries and network aggregation in microfluidic drops had been observed by microscopy [57], [14, 15].

PDMS-capillary composite microfluidic devices (see Fig. 11a) were developed and used for the experiments. These devices served two purposes: controlled water-in-oil droplet generation in the PDMS part and X-ray compatibility of the glass capillary. One great advantage of using microfluidics for studying protein systems and flowing the biological

material by the X-ray beam is that radiation damage is substantially reduced.

The three aqueous inlets 1, 2, 3 were used to mix vimentin with the K^+ ions separated by a stream of buffer. The droplets were then pinched off by the oil phase flow (inlet 4) from adjacent directions [57], [14]. These droplets then flowed down the outlet channel into the quartz capillary. Data were taken at several positions along the capillary enabling us to convert the spatial resolution into time resolution and reaching a time resolution of milliseconds. We performed two different sets of experiments: first, at Elettra/Trieste we employed long exposure times of 10 minutes and thereby averaged over many drops. The beam spot was defined by a 50 μm diameter pinhole to fit in the capillary (inner diameter 80 μm) and avoid streaks stemming from the capillary edges. The data were collected using a PILATUS 1M single-photon counting pixel detector. First results of such a measurement are shown in Fig. 11b, where SAXS curves for different time points in the assembly process are shown. Second, at ESRF/ID13 short exposure times of 10 ms with 3 ms dead time were employed. We used a micro-focused X-ray beam with dimensions of 5 μm $\times$ 5 μm, which was incident at different points on the capillary whilst the droplets (dimension of about $\sim$ 120 μm $\times$ 80 μm (h $\times$ v)) flowed by. The data were collected using a MAXIPIX single-photon counting pixel detector, which can acquire with a high frame rate. Due to the small beam size and the short exposure time, several acquisitions per flowing droplet were possible ($\sim 22 - 26$ exposures). This strategy allowed us to distinguish clearly between the aqueous (red) and oil (blue) phase (see Fig. 11c). As the oil absorbs the X rays more strongly than the aqueous phase, the higher scattering intensity can be attributed to signal from inside the drops. In order to increase the signal-to-noise ratio, we averaged the signal from the aqueous droplets only, while discarding the signal from the oil.

With this experiment, we have demonstrated that the study of assembly and aggregation with droplets in flow by X-ray methods is feasible and time scales accessible range from milliseconds to seconds, which is exactly what we need to understand the assembly of biological macromolecules.

1.11 Implementation of a New Sample Stage for HORST (AG Rosenhahn)

The sample stage previously employed for ptychographic and full-field zone plate microscopy in combination with small angle X-ray scattering proved to be prone to mechanical vibrations and drift. In order to achieve the maximum spatial resolution during microscopic measurements, these mechanical instabilities had to be eliminated. Therefore, a new stage design (Fig. 12a) was developed and optimized with regard to optimal mechanical stability using computer simulations (COMSOL Multiphysics). During first beamtimes the superior stability of the new stage design has been experimentally confirmed. The two stacked single-axis piezo stages employed for fine scanning of the sample during the ptychographic scans has been replaced with an integrated 3-axis piezo system with shorter travel ranges but increased mechanical load capacity. As example two

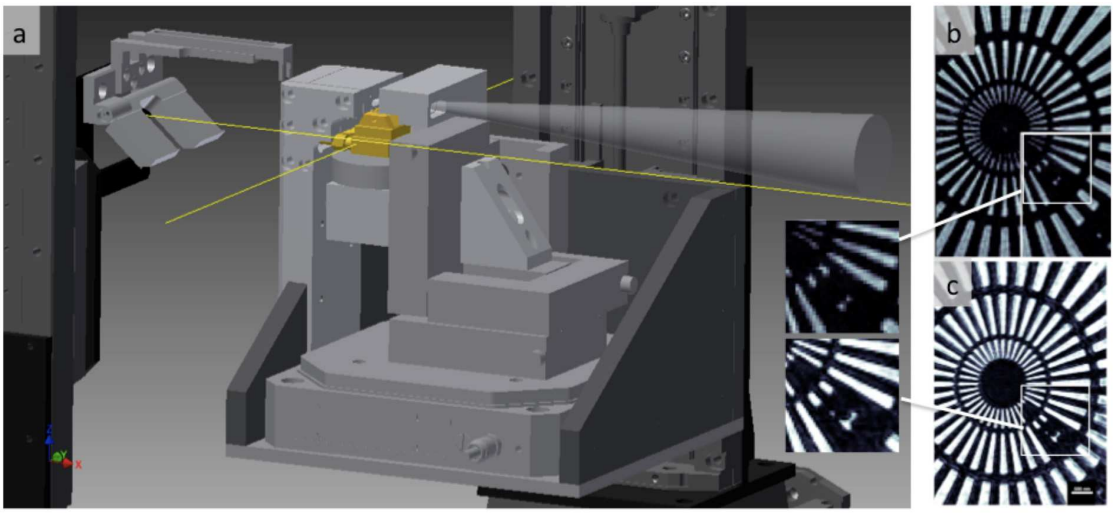

Figure 12: CAD representation of the new sample stage for combined ptychographic and full-field microscopy as well as small angle X-ray scattering of cryogenic samples. The new design has been optimized by simulation for maximum mechanical stability. The stack of two single-axis piezo stages previously used for scanning the sample in the ptychography mode has been replaced by an integrated 3-axis piezo system with increased tolerance for mechanical load. b) Previous reconstruction of a ptychographic scan with lower mechanical stability. c) Reconstruction from Ptychographic scan with new setup. Innermost ring of the test chart: 50 nm.

reconstructions from ptychographic scans are shown in Figure 12b) from an old scan [58] and c) from a scan with the new setup. The resolution of the innermost ring (50 nm test pattern) was enhanced and a resolution of $\approx$ 35 nm is now reached. Especially vibrations previously visible during full-field microscopy acquisitions have now been reduced significantly, while the versatile application options could be preserved. Using the new stage it is possible to perform ptychography scans, full-field microscopy using Fresnel zone-plates, small angle X-ray scattering and x-ray absorption spectroscopy on the same sample, either in the cryogenic or in the dried state. The new stage design is fully compatible with the chamber's load-lock system [16] enabling a sample exchange within minutes.

1.12 A Micro-Patterned Silicon Chip as Sample Holder for Macromolecular Crystallography Experiments with Minimal Background Scattering (AG Meents)

For structural investigations of micrometer sized samples with X rays sample efficient delivery remains a challenge. In particular for very small samples background scattering from conventional sample holders reduces the achievable signal to noise ratio and thereby

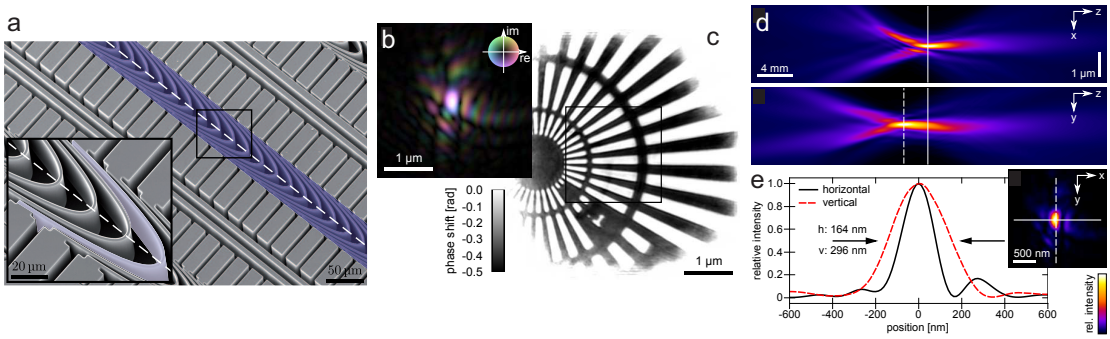

Figure 13: a) Electron micrograph of refractive lamellar lenses (RLL) made of silicon an aluminum oxide. b) and c) characterization of the nano-beam profile by ptychographic imaging of a test pattern. d) horizontal and vertical caustic of the nanobeam generated by two crossed RLLs. e) Intensity profile at the finely dashed line in d).

the achievable resolution, it is often difficult to locate the small samples. To solve this problem we have developed a micro-fabricated sample holder from single crystalline silicon with micropores, which carries up to thousands of samples and does not contribute to background scattering. For loading, the suspended particles are pipetted onto the chip and the suspending liquid is subsequently soaked off through the micropores. Particles larger than the pore size are retained and arrange themselves according to the micropore pattern. We have tested our chip with protein microcrystals and were able to collect 1.5 Å high resolution diffraction data from crystals with sizes of 4 micrometers and smaller. Due to its good thermal conductivity the chip is ideal suited for future in-vacuum experiments with biological samples which require cryo-cooling to prevent the samples from dehydration. This development was recently published in [17].

1.13 Hard X-ray Nanofocusing by Refractive Lenses of Constant Thickness (AG Schroer)

In order to focus light or x rays, the thickness of a refractive lens is typically varied over its aperture. To eventually improve the transmission and numerical aperture of refractive lenses, we developed a refractive X-ray lens made of lamellae of constant thickness, a so-called refractive lamellar lens [RLL, Fig. 13a)]. Refractive power is created by a specific bending of the lamellae rather than by a concave lens profile. This very special design has the technological advantage that materials like sapphire or diamond can be used to make lenses by coating techniques. These materials promise a higher transmission and improved numerical aperture that lead to brighter and smaller hard X-ray nanobeams. We characterized these optics by ptychography of a test object in the hard X-ray scanning microscope at P06 of PETRA III [Fig. 13b)]. A first lens prototype made of silicon coated with aluminum oxide focused x rays with a photon energy $E = 15.25$ keV to a lateral beam size of 164×296 nm full width at half maximum. This work was published in

[26].

2 Erreichte Meilensteine

Most of the milestones in 2014 have been reached, with a few exceptions. One important factor that led to some delays was the shutdown of PETRA III from early 2014 to spring 2015. Where possible, experiments were transferred to other synchrotron radiation sources. The shutdown, however, had also some advantages: instrumental improvements could be carried out more easily, leading to improved experimental conditions in 2015.

In the following, we discuss the progress and comment on the individual milestones:

Cell3 (year 3) model organisms and first test of live cell imaging: milestone reached (cf. section 1.4).

Mem3a (year 3) synaptic vesicles in microfluidic channels interacting with lipid bilayers of liposomes, probed by nanoscale diffraction. This topic was postponed. The milestone is not reached.

Mem3b (year 3) nanoscale diffraction on membranes in microfluidic chambers has been carried out (milestone reached). Significant work on testing different microfluidic chambers has been performed, including adaptations of commercial one. We have decided to concentrate all efforts on cellular imaging and diffraction, and optimize the setting of P10 for these experiments, including beam preparation, fast scanning, ptychographic and holographic imaging. Since this topic is particularly timely, live-cell imaging has been a major emphasis, which has now been realized for several systems and contrast modes, including holographic imaging of bacterial cells and macrophages during phagocytatosis.

Mel3 (year 3) imaging of frozen hydrated melanosomes: frozen hydrated melanosomes were successfully imaged at P10 in a frozen hydrated state. (milestone reached)

Alg3 (year 3) investigation of frozen-hydrated marine biofouling organisms and cells: frozen-hydrated diatoms and bacterial cells were successfully imaged with ptychographic and zone-plate imaging at BESSY. (milestone reached)

Cat3 (year 3) *in-situ* study of the ignition of the catalytic partial oxidation of methane around a single catalyst particle. This milestone is not yet fully reached, as no beamtime was allocated for single-particle analysis. The *in-situ* microreactors were successfully fabricated (cf. CatRe3) and the ptychographic imaging techniques were improved to have sufficient sensitivity and resolution. First *in-situ* experiments were carried out, studying the annealing of nanoparticles and nanoporous materials (cf. sections 1.7 and 1.8).

Mfluid3 (year 3) microfluidic devices for use in beamlines P06, P10 and P11: we tested our microfluidic devices at P10; we were, unfortunately not successful yet at P11 and still have to work on this point. We did not get beamtime for measurements at P06 and will try again in the next beamtime proposal round. (Milestone reached for P10)

CatRe3 (year 3) *in-situ* reactor for 2D study of catalytic reactions. Two types of chemical microreactors were realized for catalysis (gas flow) and *in-situ* liquid cell. For the first prototype of the gas phase microreactor, temperature stability and homogeneity were not optimal. Therefore, improvements were made, leading to a second generation of microreactors. The second generation shows a high temperature homogeneity and stability and is well suited for reactions like CO oxidation, the catalytic partial oxidation (CPO) of methane or the selective catalytic reduction (SCR) of NO_x. The latter reactions have already been studied in this reactor.

Mdiff3 (year 3) cryogenic micro-diffraction experiments on melanosomes and cytoskeleton of cells. Due to the one-year shutdown of PETRA III, this milestone could not be reached in 2014. It is now foreseen for 2015 when PETRA III resumes operation.

Theo2 (year 2) model of partially coherent nanobeams. Milestone reached in 2013 [18].

Theo3 (year 3) improved ptychographic reconstruction, taking mechanical instabilities into account. Several algorithms were developed that cope with different types of instability [59, 60]. Milestone reached in 2013.

3 Einhaltung des Finanzierungs- und Zeitplans

The group at TU Dresden has in parts moved to DESY in Hamburg (cf. below). However, the virtual institute remains in Dresden. There are no changes to the organizational structure of the VI.

Currently, the project is within the financial and time plan.

4 Publikationen, Vorträge, Preise etc. bitte gegebenenfalls als Anhang beifügen

4.1 Berufung:

In 2014, Christian Schroer was appointed leading scientist for PETRA III at DESY and full professor for X-Ray Nanoscience and X-Ray Optics at the University of Hamburg.

His group has moved in parts from TU Dresden to Hamburg, however, the TU Dresden part of the VI remains in Dresden.

4.2 Meetings & Outreach into the Scientific Community:

A satellite workshop to the DESY Photon Science Users Meeting in Hamburg was organized by the VI-403. It is already the 4th workshop held in the context of the Users Meeting entitled "4th Workshop on X-Ray Nano-Imaging of Biological and Chemical Systems at PETRA III". It aimed at the Photon Science user community interested in nano imaging, giving an overview over the possibilities of nano imaging at the x-ray microscopes at PETRA III (cf. group photo below). The workshop was well attended with over 80 participants.

4.3 Oral Presentations:

- C. Schroer, "PETRA III: Highly Brilliant Photons for Nano Science," ANST-2014, Kolkata, India, Dec. 12, 2014 (invited)
- S. Köster, "Physical properties of biological polymers — from self-assembly to networks in cells"; Universität Paderborn, November 24, 2014 (invited)
- C. Schroer, "The Future of Science at Synchrotron Radiation Sources," 50 Photon Years, DESY, Hamburg, Oct. 28, 2014 (keynote lecture)

- C. Schroer, "X-Ray Microscopy: Sharp Views into the Nano Cosmos," PIER Colloquium, Hamburg, Oct. 17, 2014
- C. Schroer, "Faszination Synchrotronstrahlung: Lichtblick in die Nanowelt," SNI 2014, Bonn, Germany, Sept. 23, 2014 (keynote lecture)
- J. Reinhardt, "Hochauflösende Bildgebung mit chemischem Kontrast durch Ptychographie," SNI 2014, Bonn, Germany, Sept. 21-23, 2014
- A. Gänzler, "Kombination von QEXAFS, Infrarot-Thermographie und katalytischer Aktivität zur Untersuchung eines Autoabgaskatalysators während oszillierendem Umsatz," SNI 2014, Bonn, Sept. 21-23, 2014
- A. Rosenhahn, "Ultrastructure of biological systems probed by X-rays," SNI 2014, Bonn, Germany, Sept. 22, 2014
- C. Schroer, "Microscopy with Coherent X Rays," APS Upgrade Workshop on Coherent Imaging, Evanston, USA, Sept. 6, 2014 (invited)
- C. Schroer, "Microscopy with Coherent X Rays: Toward 1 nm Resolution and Beyond," Coherence 2014, Evanston, USA, Sept. 2, 2014 (invited)
- C. Schroer, "Hard X-Ray Nanofocusing at Low-Emittance Synchrotron Radiation Sources," APS, Argonne, Aug. 28, 2014
- A. Gänzler, "Chasing active sites: In operando investigations on a Pt/Al_2O_3 catalyst during isothermal CO oscillations," ICEC 2014, Asheville, North Carolina, USA, Aug. 24-27, 2014
- D. E. Doronkin, "Spatially- and time-resolved XAS and V2C XES of zeolite catalysts during NO_x-SCR," ICEC 2014, Asheville, North Carolina, USA, Aug. 24-27, 2014
- S. Köster, "X-ray imaging of biological matter using microfluidics", ESRF, Grenoble, June 19, 2014 (invited)
- A. Gänzler, "Pt-based Diesel Oxidation Catalysts: Oxidation state of Platinum and the origin of CO oscillations in real Pt/Al_2O_3 catalysts," Nordic Catalysis symposium, Oslo, Norway, June 15-17, 2014
- A. Rosenhahn, "Surface selection and settlement of marine biofouling organisms," European Adhesion Conference, Alicante, Spain, April 24, 2014 (keynote lecture)
- J.-D. Grunwaldt, "Nanomaterials at work: Insight into catalysts and sensors by synchrotron-based techniques," Symposium AAA: Application of In-Situ Synchrotron Radiation in Nanomaterials Research, MRS Spring Meeting 2014, San Francisco, USA, April 21-24, 2014 (keynote lecture)
- S. Köster, "Intermediate Filaments — mechanical building blocks and dynamic elements of the cell", DPG Spring Meeting, Berlin, April 2, 2014 (invited)

- D. E. Doronkin, "Spatially- and time-resolved XAS of zeolite catalysts during NO_x-SCR," LeStudium conference "Heterogeneous catalysis: recent advances in preparation and characterization," Orleans, USA, March 31-April 1, 2014 (invited)
- C. Schroer, "High-resolution x-ray imaging at synchrotron radiation sources and XFELs," Symposium Crystallography in Materials Science (SYCM), DPG Tagung, Dresden, March 31, 2014 (invited)
- S. Köster, "X-ray studies of biological matter — from micro-SAXS to nano-imaging", University of Copenhagen, Denmark, March 14, 2014 (invited)
- S. Köster, "X-ray studies of biological matter — from micro-SAXS to nano-imaging"; Paul Scherrer Institut, Villigen, Switzerland, Feb. 28, 2014 (invited)
- C. Schroer, "High-Resolution X-Ray Imaging at Synchrotron Radiation Sources and XFELs," X-ray Science Workshop, Helmholtz Institute Jena, Feb. 26., 2014
- C. Schroer, "X-Ray Nano-Imaging of Biological and Chemical Systems at PETRA III," 4. Satellite Workshop at the DESY Photon Science Users' Meeting, Jan. 30, 2014
- G. Hofmann, "Quasi in situ X-Ray Tomography on Exhaust Gas Catalysts: Quantification of Ageing Effects," German Engineering Materials Science Centre (GEMS) Satellite Workshop at DESY Photon Science Users' Meeting, Jan. 30, 2014 (invited)
- S. Köster, "Self-assembly if intermediate filaments in the presence of counter ions", International Symposium on Polyelectrolytes, En Gedi, Israel, Jan. 21, 2014 (invited)
- A. Rosenhahn, "Surface cues relevant for marine biofouling," GDCh Colloquium, University of Paderborn, Jan. 20, 2014 (invited)
- C. Schroer, "Abbilden ohne Optik: Mikroskopie mit kohärenter Röntgenstrahlung," Physikkolloquium, Universität Regensburg, Jan. 13, 2014
- S. Köster, "X-ray studies of biological matter — from micro-SAXS to nano-imaging", Institut für Strukturphysik, TU Dresden, Jan. 7, 2014 (invited)

4.4 Technology Transfer

In 2014 **Suna Precision GmbH** (http://www.suna-precision.com) was founded by one of the members of the VI (A. Meents) as a spin-off company of DESY. Suna Precision commercializes high-precision mechanical systems for nano-positioning, automation, and synchrotron radiation instrumentation.

4.5 Outreach

- C. Schroer, "Microscopy with Coherent X Rays," Cheiron School 2014, SPring-8, Harima, Japan, Sept. 29, 2014
- S. Baier (AG Grunwaldt) gave a lecture for 16 high school students on X-ray microscopy at the Chemie-Olympiade at KIT in Karlsruhe (Sept. 2014).
- C. Schroer, "X-Ray Microscopy with Coherent Radiation: Ptychography," Debye Spring School, University of Utrecht, Apr. 10, 2014
- C. Schroer, "X-Ray Microscopy," Course on Modern Concepts and spectroscopic methods in materials science and catalysis, KIT, 18. Feb., 2014
- J.-D. Grunwaldt, "Fahrt in die Welt der Katalyse," FChO-Workshop, Münster, Jan 3-6, 2014 (oral presentation)

Publications in the Reporting Period

[1] D. Dzhigaev, U. Lorenz, R. P. Kurta, F. Seiboth, T. Stankevic, S. Mickevicius, A. Singer, A. Shabelin, O. M. Yefanov, M. N. Strikhanov, G. Falkenberg, C. G. Schroer, R. Feidenhans'l, and I. A. Vartanyants, J. Phys. Conf. Ser. **499**, 012020 (2014).

[2] B. Weinhausen, O. Saldanha, R. N. Wilke, C. Dammann, M. Priebe, M. Burghammer, M. Sprung, and S. Köster, Phys. Rev. Lett. **112**, 088102 (2014), research Highlight in Nature Materials 13, 323 (2014).

[3] V. Piazza, B. Weinhausen, A. Diaz, C. Dammann, C. Maurer, M. Reynolds, M. Burghammer, and S. Köster, ACS Nano **8**, 12228 (2014).

[4] T. Reusch, F. J. R. Schülein, J. D. Nicolas, M. Osterhoff, A. Beerlink, H. J. Krenner, M. Müller, A. Wixforth, and T. Salditt, Phys. Rev. Lett. **113**, 118102 (2014).

[5] T. Reusch, M. Osterhoff, J. Agricola, and T. Salditt, J. Synchrotron Rad. **21**, 708 (2014).

[6] J.-D. Nicolas, T. Reusch, M. Osterhoff, M. Sprung, F. J. R. Schülein, H. J. Krenner, A. Wixforth, and T. Salditt, J. Appl. Cryst. **47**, 1596 (2014).

[7] M. Bartels, M. Krenkel, J. Haber, R. N. Wilke, and T. Salditt, Phys. Rev. Lett. **114**, 048103 (2015).

[8] T. Gorniak, T. Haraszti, H. Suhonen, Y. Yang, A. Hedberg-Buenz, D. Koehn, R. Heine, M. Grunze, A. Rosenhahn, and M. G. Anderson, Pigment Cell & Melanoma Research **27**, 831 (2014).

[9] D. Doronkin, M. Casapu, T. Günter, O. Müller, R. Frahm, and J.-D. Grunwaldt, J. Phys. Chem. C **118**, 10204 (2014).

[10] G. Hofmann, A. Rochet, S. Baier, M. Casapu, S. Ritter, F. Wilde, M. Ogurreck, F. Beckmann, and J.-D. Grunwaldt, J. Phys. Conf. Ser. **499**, 012017 (2014).

[11] J. Wallentin, M. Osterhoff, R. N. Wilke, K.-M. Persson, L.-E. Wernersson, M. Sprung, and T. Salditt, Nano Lett. **14**, 7071 (2014).

[12] Z. Huang, M. Bartels, R. Xu, M. Osterhoff, S. Kalbfleisch, M. Sprung, A. Suzuki, Y. Takahashi, T. Blanton, T. Salditt, and J. Miao, Nature Materials (2015), accepted for publication.

[13] M. E. Brennich, S. Bauch, U. Vainio, T. Wedig, H. Herrmann, and S. Köster, Soft Matter **10**, 2059 (2014).

[14] C. Dammann and S. Köster, Lab on a Chip **14**, 2681 (2014).

[15] C. Dammann, H. Herrmann, and S. Köster, Israel J. Chem. (2015), DOI: 10.1002/ijch.201400153.

[16] T. Gorniak and A. Rosenhahn, Zeitschift für Physikalische Chemie **228**, 1089 (2014).

[17] P. Roedig, I. Vartiainen, R. Duman, S. Panneerselvam, N. Stübe, O. Lorbeer, M. Warmer, G. Sutton, D. I. Stuart, E. Weckert, C. David, A. Wagner, and A. Meents, Scientific Reports **5**, 10451 (2015).

[18] A. Singer and I. A. Vartanyants, J. Synchrotron Rad. **21**, 5 (2014).

[19] T. Gorniak, T. Haraszti, V. M. Garamus, A. R. Buck, T. Senkbeil, M. Priebe, A. Hedberg-Buenz, D. Koehn, T. Salditt, M. Grunze, M. G. Anderson, and A. Rosenhahn, PLoS ONE **9**, e90884 (2014).

[20] M. Brennich and S. Köster, Microfluidics and Nanofluidics **16**, 39 (2014).

[21] A. V. Zozulya, A. Shabalin, H. Schulte-Schrepping, J. Heuer, M. Spiwek, I. Sergeev, I. Besedin, I. A. Vartanyants, and M. Sprung, J. Phys. Conf. Ser. **499**, 012003 (2014).

[22] R. P. Kurta, L. Grodd, E. Mikayelyan, O. Y. Gorobtsov, I. Fratoddi, I. Venditti, M. Sprung, S. Grigorian, and I. A. Vartanyants, J. Phys. Conf. Ser. **499**, 012021 (2014).

[23] P. Skopintsev, A. Singer, J. Bach, L. Müller, B. Beyersdorff, S. Schleitzer, O. Gorobtsov, A. Shabalin, R. P. Kurta, D. Dzhigaev, O. M. Yefanov, L. Glaser, A. Sakdinawat, G. Grübel, R. Frömter, H. P. Oepen, J. Viefhaus, and I. A. Vartanyants, J. Synchrotron Rad. **21**, 722 (2014).

[24] J.-M. Meijer, A. Shabalin, R. Dronyak, O. M. Yefanov, A. Singer, R. P. Kurta, U. Lorenz, O. Gorobstov, D. Dzhigaev, J. Gulden, D. V. Byelov, A. V. Zozulya, M. Sprung, I. A. Vartanyants, and A. V. Petukhov, J. Appl. Cryst. **47**, 1199 (2014).

[25] A. Singer, U. Lorenz, A. Marras, A. Klyuev, J. Becker, K. Schlage, P. Skopintsev, O. Gorobtsov, A. Shabalin, H.-C. Wille, H. Franz, H. Graafsma, and I. A. Vartanyants, Phys. Rev. Lett. **113**, 064801 (2014).

[26] F. Seiboth, M. Scholz, J. Patommel, R. Hoppe, F. Wittwer, J. Reinhardt, J. Seidel, M. Knaut, A. Jahn, K. Richter, J. W. Bartha, G. Falkenberg, and C. G. Schroer, Appl. Phys. Lett. **105**, 131110 (2014).

[27] C. G. Schroer and G. Falkenberg, J. Synchrotron Rad. **21**, 996 (2014).

References

[28] B. Weinhausen, J.-F. Nolting, C. Olendrowitz, J. Langfahl-Klabes, M. Raynolds, T. Salditt, and S. Köster, New J. Phys. **14**, 085013 (2012).

[29] B. Weinhausen and S. Köster, Lab on a Chip **13**, 212 (2013).

[30] J. Kayser, H. Grabmayr, M. Harasim, H. Herrmann, and A. R. Bausch, Soft Matter **8**, 8873 (2012).

[31] T. Reusch, F. Schülein, C. Bömer, M. Osterhoff, A. Beerlink, H. J. Krenner, A. Wixforth, and T. Salditt, AIP Advances **3**, 072127 (2013).

[32] J. D. Simon and D. N. Peles, Acc. Chem. Res. **43**, 1452 (2010).

[33] J. D. Simon, D. Peles, K. Wakamatsu, and S. Ito, Pigment Cell & Melanoma Research **22**, 563 (2009).

[34] S. Ito and K. Wakamatsu, Pigm. Cell Res. **16**, 523 (2003).

[35] G. Agrup, C. Hansson, H. Rorsman, and E. Rosengren, Arch. Dermatol. Res. **272**, 103 (1982).

[36] S. Ito and K. Wakamatsu, Photochemistry and Photobiology **84**, 582 (2008).

[37] D. N. Peles, L. Hong, D.-N. Hu, S. Ito, R. J. Nemanich, and J. D. Simon, J. Phys. Chem. B **113**, 11346 (2009).

[38] G. Martínez-Criado, R. Tucoulou, P. Cloetens, P. Bleuet, S. Bohic, J. Cauzid, I. Kieffer, E. Kosior, S. Labouré, S. Petitgirard, A. Rack, J. A. Sans, J. Segura-Ruiz, H. Suhonen, J. Susini, and J. Villanova, J. Synchrotron Rad. **19**, 10 (2011).

[39] R. E. W. Hancock, Nature Reviews Drug Discovery **6**, 28 (2007).

[40] D. J. Payne, M. N. Gwynn, D. J. Holmes, and D. L. Pompliano, Nature Reviews Drug Discovery **6**, 29 (2007).

[41] G. L. Hura, A. L. Menon, M. Hammel, R. P. Rambo, F. L. Poole II, S. E. Tsutakawa, F. E. Jenney Jr., S. Classen, K. A. Frankel, R. C. Hopkins, S. jae Yand, J. W. Scott, B. D. Dillard, M. W. W. Adams, and J. A. Tainer, Nature Methods **6**, 606 (2009).

[42] K. Hilpert, R. Volkmer-Engert, T. Walter, and R. E. W. Hancock, Nature Biotechnology **23**, 1008 (2005).

[43] S. Baier, A. Rochet, G. Hofmann, M. Kraut, and J.-D. Grunwaldt, Rev. Sci. Instrum. **86**, 065101 (2015).

[44] J.-D. Grunwaldt, J. B. Wagner, and R. E. Dunin-Borkowski, Chem. Cat. Chem. **5**, 62 (2013).

[45] J.-D. Grunwaldt, B. Kimmerle, A. Baiker, P. Boye, C. G. Schroer, P. Glatzel, C. N. Borca, and F. Beckmann, Catalysis Today **145**, 267 (2009).

[46] A. M. Beale, S. D. M. Jacques, and B. M. Weckhuysen, Chem. Soc. Rev. **39**, 4656 (2010).

[47] B. C. Enger, R. Lødeng, and A. Holmen, Appl. Catal. A: Gen. **346**, 1 (2008).

[48] J.-D. Grunwaldt, S. Hannemann, C. G. Schroer, and A. Baiker, J. Phys. Chem. B **110**, 8674 (2006).

[49] A. M. Gänzler, M. Casapu, A. Boubnov, O. Müller, H. Lichtenberg, and J.-D. Grunwaldt, J. Catal. (2015), accepted for publication.

[50] G. Hofmann, A. Rochet, E. Ogel, M. Casapu, S. Ritter, M. Ogurreck, and J.-D. Grunwaldt, RSC Adv. **5**, 6893 (2015).

[51] J. M. Thomas and J.-C. Hernandez-Garrido, Angew. Chem. Int. Ed. **48**, 3904 (2009).

[52] J.-D. Grunwaldt and C. G. Schroer, Chem. Soc. Rev. **39**, 4741 (2010).

[53] A. M. Kiss, W. M. Harris, A. Nakajo, S. Wang, J. Vila-Comamala, A. Deriy, and W. K. S. Chiu, Microsc. Micoanal. **21**, 290 (2015).

[54] S. Baier, C. D. Damsgaard, M. Scholz, F. Benzi, A. Rochet, R. Hoppe, T. Scherer, J. Shi, A. Wittstock, M. Burghammer, J. B. Wagner, C. G. Schroer, and J.-D. Grunwaldt, Microsc. Micoanal. (2015), to be published.

[55] K. Høydalsvik, J. B. Fløystad, T. Zhao, M. Esmaeili, A. Diaz, J. W. Andreasen, R. H. Mathiesen, M. Rønning, and D. W. Breiby, Appl. Phys. Lett. **104**, 241909 (2014).

[56] M. E. Brennich, J.-F. Nolting, C. Dammann, B. Nöding, S. Bauch, H. Herrmann, T. Pfohl, and S. Köster, Lab on a Chip **11**, 708 (2011).

[57] C. Dammann, B. Nöding, and S. Köster, Biomicrofluidics **6**, 022009 (2012).

[58] K. Giewekemeyer, M. Beckers, T. Gorniak, M. Grunze, T. Salditt, and A. Rosenhahn, Opt. Express **19**, 1037 (2011).

[59] A. Schropp, R. Hoppe, V. Meier, J. Patommel, F. Seiboth, H. J. Lee, B. Nagler, E. C. Galtier, B. Arnold, U. Zastrau, J. B. Hastings, D. Nilsson, F. Uhlen, U. Vogt, H. M. Hertz, and C. G. Schroer, Scientific Reports **3**, 1633 (2013).

[60] M. Beckers, T. Senkbeil, T. Gorniak, K. Giewekemeyer, T. Salditt, and A. Rosenhahn, Ultramicroscopy **126**, 44 (2013).